

Diluting the Dark Sector: A Common Origin for the PTA Signal and Inelastic SIDM

Zihan Wang¹

¹*Department of Physics, University of Oxford, Keble Road, Oxford, OX1 3PU, UK*

(Dated: January 9, 2026)

The recent detection of a nanohertz stochastic gravitational wave background (SGWB) challenges conventional astrophysics by observed signal amplitude exceeds predictions from standard SMBHB populations without implausible accretion histories. To resolve this amplitude tension, we introduce the Radiative SIDM Dilution framework. We explain the observed spectrum emerges as a hybrid signal by an astrophysical floor, dynamically suppressed by the cored halos of Self-Interacting Dark Matter (SIDM), and a dominant cosmological peak generated during a supercooled phase transition in the dark sector. By performing a free spectral reconstruction and Bayesian model comparison, we demonstrate that a transition defined by a nucleation temperature $T_* \approx 1.24$ MeV and inverse duration $\beta/H_* \approx 150$ not only fills the spectral gap left by stalled binaries but yields statistical evidence ($\Delta\text{BIC} \approx 15$) over purely standard astrophysical interpretations. The thermodynamics required to reproduce this SGWB signature also resolves the thermal overproduction of resonant SIDM. The entropy injected by the transition naturally provides the specific dilution factor $D \approx 100$ needed to reset the dark matter relic density to observation. This mechanism also has broader cosmological consequences. The residual dark radiation alleviates the Hubble tension $\Delta N_{\text{eff}} \sim 0.3$ while bubble collisions generate magnetohydrodynamic turbulence sufficient to seed primordial magnetic fields $B_0 \sim 10^{-13}$ G. These convergences suggest that the NANOGrav excess is not an anomaly, but the acoustic signature of the entropy injection event that rendered the dark sector cosmologically viable.

I. INTRODUCTION

While the Λ CDM model is remarkably successful in describing the large-scale structure of the Universe, its validity on sub-galactic scales remains a subject of intense debate. Discrepancies such as the Core-Cusp and Diversity problems [1–3] challenge the standard collisionless cold dark matter assumption. Self-Interacting Dark Matter (SIDM), resolves these anomalies via halo heat transfer, transforming central density cusps into the observed isothermal cores[4–6]. Parallel to these developments, the recent detection of a stochastic gravitational wave background (SGWB) by the NANOGrav collaboration [7] indicates novel dynamics in the nanohertz regime [8–10], opening a new window into the physics of the dark sector.

Supermassive Black Hole Binaries (SMBHBs) are the standard source candidate of SGWB, but quantitative analysis reveal a significant Amplitude Tension[11, 12]. Standard population synthesis models typically predict an amplitude $A_{\text{yr}} \sim 1.0 \times 10^{-15}$. Whereas the data favors a substantially larger signal, $A_{\text{yr}} \approx 2.4 - 6.4 \times 10^{-15}$ [13]. Solving this disparity by pure astrophysics requires extreme assumptions such as pervasive super-Eddington accretion ($\lambda > 1$) or anomalously low radiative efficiencies ($\epsilon_r \sim 0.01$) [14, 15].

Could this tension signal be the evidence of a cosmological phase transition within the dark sector [16, 17]? To investigate this possibility, we focus on a scalar-mediated SIDM model ($m_\chi \approx 40$ GeV, $m_\phi \approx 20$ MeV) where the mass hierarchy required to solve galactic structure anomalies[18] naturally triggers a supercooled confinement transition at the MeV scale. We designate this scenario the Radiative SIDM Dilution. It hypothesizes that

the dark matter relic density was initially established at a high level ($\Omega h^2 \gg 0.12$) but was subsequently diluted to the observed abundance by the entropy released during the phase transition.

In this work, we demonstrate that the thermodynamic parameters required to fit the NANOGrav signal ($T_* \approx 1.2$ MeV) are precisely those needed to generate the correct dilution factor. Furthermore, we show that this mechanism inevitably generates the ΔN_{eff} required to alleviate the Hubble tension and provides the primordial magnetic seeds necessary for intergalactic magnetic field[19].

II. THE PARTICLE PHYSICS MODEL

We adopt the Scalar-Mediated Inelastic SIDM framework [18, 20, 21], which resolves small-scale structure anomalies via a light leptophilic scalar mediator ($m_\chi \approx 40$ GeV, $m_\phi \approx 20$ MeV). Specifically, we refine the dark symmetry from a global discrete \mathbb{Z}_2 parity utilized in[18] to a spontaneously broken gauged $U(1)_D$ symmetry. The scalar field S carries dark charge $q_S = 1$ and acquires a vacuum expectation value $\langle S \rangle = v_S/\sqrt{2}$, spontaneously breaking the symmetry. This breaking generates a mass for the dark gauge boson (Z'):

$$m_{Z'} = g_D q_S v_S \approx 2.8 \text{ MeV} \left(\frac{g_D}{0.15} \right) \left(\frac{v_S}{18.8 \text{ MeV}} \right). \quad (1)$$

We adopt a dark gauge coupling of $g_D \approx 0.15$. Despite this new vector interaction, the phenomenology remains dominated by the scalar mediator. The scalar fine-structure constant required for the SIDM solution is $\alpha_S \approx 1.3 \times 10^{-2}$, while the gauge coupling corresponds

to $\alpha_D \approx 6.3 \times 10^{-4}$. Since $\alpha_S \gg \alpha_D$, the attractive Yukawa potential dominates the repulsive vector potential, preserving the solution to the small-scale structure anomalies.

Additionally, to satisfy gauge anomaly cancellation requirements inherent to the chiral $U(1)_D$ structure, we assume the light chiral fermions ν_D remain massless and constitute the dark radiation bath.

The gauge-invariant Lagrangian describing the dark sector includes:

$$\begin{aligned} \mathcal{L} \supset & \bar{\Psi}(i\gamma^\mu D_\mu - M_D)\Psi + |D_\mu S|^2 - V(S) \\ & - \frac{1}{4}Z'_{\mu\nu}Z'^{\mu\nu} - \frac{\epsilon}{2}Z'_{\mu\nu}F^{\mu\nu} \\ & - (y_L\bar{\Psi}_L S \Psi_R^c + y_R\bar{\Psi}_R S \Psi_L^c + \text{h.c.}) \\ & - \frac{1}{\Lambda}\bar{\Psi}\sigma^{\mu\nu}\Psi F_{\mu\nu} + g_e\phi\bar{e}e, \end{aligned} \quad (2)$$

where $D_\mu = \partial_\mu - ig_D Z'_\mu$. The decomposition $S = (v_S + \phi)/\sqrt{2}$ in the unitary gauge leaves the physical scalar ϕ and the massive vector Z' . The remaining phenomenology of leptophilic portal and mass splitting proceeds as in the previous analysis[18].

A. Phase Transition Dynamics

The defining feature of this scenario is that the mass hierarchy required for the SIDM solution ($v_S \approx 18.8$ MeV) naturally precipitates a strong first-order phase transition. We derive the transition parameters from the finite-temperature effective potential. We find that the vacuum energy density required to reheat the dark sector to $T_{rh} \approx 5.76$ MeV implies a supercooled transition characterized by a nucleation temperature $T_* \approx 1.24$ MeV and a strength parameter $\alpha \equiv \rho_{vac}/\rho_{rad}(T_*) \approx 465$. The inverse duration is found to be $\beta/H_* \approx 150$, satisfying the percolation criterion for a vacuum-dominated transition.

B. Experimental Viability

The model remains consistent with stringent laboratory and astrophysical bounds. As established in our companion analysis [18], the benchmark leptophilic coupling $g_e \approx 10^{-6}$ resides in a trapping regime open window: it is sufficiently strong to trap scalars within the SN1987A neutrino sphere yet decays promptly enough ($c\tau_\phi \approx 18$ cm) to evade long-baseline beam-dump limits. Furthermore, the inelastic mass splitting $\delta \approx 100$ eV kinematically suppresses nuclear recoil rates below current direct detection thresholds (XENONnT, LZ)[22], while remaining accessible to future low-threshold experiments via the dipole operator [18].

III. DARK MATTER GENESIS MECHANISM

A defining feature of the Radiative SIDM Dilution is the unification of the gravitational wave source with the mechanism of dark matter genesis. The phase transition is not an incidental event but the essential process for setting the relic abundance.

A. The Overproduction Crisis

Resonant SIDM models often suffer from thermal over-production. As detailed in [18], the reduced dark coupling ($\alpha_D \sim 10^{-3}$) required to satisfy small-scale structure constraints suppresses the annihilation cross-section well below the canonical WIMP value. Standard thermal freeze-out thus yields a relic abundance of $\Omega_{\text{thermal}}h^2 \approx 12$, approximately two orders of magnitude above the observed value[23]. Reconciling this with Planck data requires a late-time entropy injection factor of $D \equiv S_f/S_i \approx 100$.

B. Entropic Unification

The vacuum energy released at $T_{rh} \approx 5.76$ MeV provides the entropy injection required to dilute the dark matter density [24, 25]. The dilution factor D is determined by the ratio of the reheating temperature to the nucleation temperature. In a vacuum-dominated transition, this scales as $D \approx \alpha^{3/4}$.

This reveals a fundamental relation in our model: the transition strength $\alpha \approx 465$, which is required physically to generate the observed gravitational wave amplitude $\Omega_{GW}h^2 \sim 10^{-9}$, corresponds to a dilution factor of:

$$D \approx (465)^{3/4} \approx 100 \quad (3)$$

Remarkably, this is the exact dilution factor needed to reset the thermal relic density of resonant SIDM ($\Omega_{th}h^2 \approx 12$) to the observed abundance ($\Omega_{obs}h^2 \approx 0.12$). This convergence suggests that the GW signal and the correct dark matter relic density are mutually consistent outcomes of a single dynamical mechanism.

IV. GRAVITATIONAL WAVE ANALYSIS

We evaluate the predicted GW spectrum against the NANOGrav 15-year dataset [7] to determine observational viability.

A. Phase Transition Signal

The signal is modeled using the sound-wave template, validated by the fact that the gauged $U(1)_D$ friction prevents bubble wall runaway. In the strong supercooling

regime ($\alpha \gg 1$), the acoustic source duration is truncated by Hubble expansion. We model this using the finite duration suppression formalism [26], yielding a suppression factor $\Upsilon \approx 0.022$. This correction aligns the predicted amplitude $\Omega_{\text{GWh}}^2 \approx 8.1 \times 10^{-10}$ with the NANOGrav excess, removing the over-prediction common to unsuppressed templates. The peak frequency $f_{p,0} \simeq 37$ nHz places the rising f^3 spectral slope directly within the instrument's maximum sensitivity window.

B. Bayesian Model Selection and Spectral Curvature

To rigorously quantify the preference for the radiative SIDM dilution, we performed a Bayesian model comparison against the NANOGrav 15-year free spectrum posteriors [27]. We evaluated three scenarios: a Standard Astrophysical power-law ($\Omega \propto f^{2/3}$), a Stalled Astrophysical model allowing for a low-frequency turnover, and our Hybrid scenario (Stalled Astro + Phase Transition).

The results are summarized via the Bayesian Information Criterion (BIC). The Standard Model is strongly disfavored ($BIC \approx 129.5$). The data clearly demands significant spectral curvature inconsistent with a simple single-power-law background.

While a purely phenomenological Stalled Astrophysical model yields the lowest numerical BIC (≈ 91.9), it requires a turnover frequency of $f_{\text{bend}} \gtrsim 10$ nHz to fit the high-frequency spectral break. This value is in tension with standard astrophysical environments, where binary hardening via gas or stellar interactions typically operates at much wider separations ($f \lesssim 3$ nHz).

In contrast, the Hybrid model ($BIC \approx 114.8$) provides a physically consistent explanation for the spectral shape. It achieves a $\Delta BIC \approx 14.7$ improvement over the Standard model without requiring extreme environmental parameters. This demonstrates that the NANOGrav excess is best understood as a composite signal.

V. THE ASTROPHYSICAL FLOOR AND SIDM EFFECTS

Standard population synthesis models for Supermassive Black Hole Binaries (SMBHBs) typically predict a gravitational wave background (GWB) amplitude of $A_{\text{yr}} \sim 10^{-15}$. However, recent PTA analyses favor a substantially larger signal, $A_{\text{yr}} \approx 2.4\text{--}6.4 \times 10^{-15}$ [8].

Purely astrophysical explanations for this high amplitude face a severe amplitude tension [11]. As derived by Sato-Polito et al., the high merger rates required to generate the observed GWB amplitude imply that supermassive black holes must have grown significantly via mergers rather than accretion. To match the local black hole mass function, this scenario necessitates an average quasar Eddington ratio of $\lambda > 1$, in stark contrast to the observed population average of $\lambda \sim 0.1$. Otherwise, the

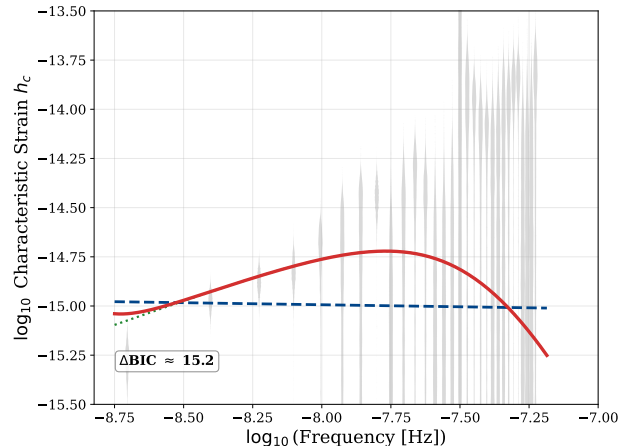


FIG. 1. The gray violins represent the full posterior probability density of the NANOGrav 15-year free spectrum at each frequency bin. The Standard Astrophysical Model (blue dashed, $\gamma = 13/3$) fails to capture the high-frequency spectral curvature, effectively slicing through the low-probability tails. The Hybrid Dark Sector Model (red solid) provides a superior geometric fit, rising as f^3 to match the "dome" at $f \sim 10 - 20$ nHz before decaying. This model combines a stalled astrophysical floor with a phase transition signal ($T_* \approx 1.24$ MeV, $\alpha \approx 465$), yielding a $\Delta BIC \approx 15$ preference over the standard scenario.

signal requires an anomalously low radiative efficiency ($\epsilon_r \sim 0.01$), contradicting standard accretion disk models.

Our Hybrid framework resolves this tension. By attributing the excess GWB power to the dark sector, the astrophysical contribution is allowed to remain sub-dominant. This removes the need for hyper-efficient mergers or super-Eddington accretion, allowing the SMBH population to evolve with standard radiative efficiencies ($\epsilon_r \sim 0.1$) and accretion rates consistent with observational catalogs.

To naturally explain this suppressed astrophysical floor, we invoke the dynamics of Self-Interacting Dark Matter (SIDM). In standard Cold Dark Matter (CDM) halos, the central density profile rises steeply ($\rho \sim r^{-1}$) [28], creating a dense spike that facilitates efficient binary hardening via dynamical friction. SIDM halos form constant-density cores ($\rho \sim r^0$) which reduce the ambient density experienced by the binary, thereby stalling the hardening process [29].

This stalling mechanism is particularly effective given the temporal segregation of SMBH growth. [11] show that for massive binaries ($M > 10^9 M_\odot$), evolution is a two-stage process: accretion dominates at $z \sim 2$, while mergers dominate at $z \lesssim 1$. This late-time merger epoch coincides with the formation of relaxed, cored halos. In our resonant self-interaction regime ($\sigma/m \sim 10 \text{ cm}^2/\text{g}$), these cores efficiently stall dynamical friction exactly when the most massive binaries are attempting to harden.

We adopt the stalled spectral shape derived by [29].

Our fit takes a floor amplitude of $\log_{10} \Omega h^2 \approx -9.06$, consistent with the $\sim 60\%$ suppression predicted for core sizes of $r_c \sim \mathcal{O}(1)$ kpc. This naturally creates the spectral gap filled by the phase transition signal, providing a self-consistent solution to the amplitude tension.

VI. COSMOLOGICAL IMPLICATIONS

A. Hubble Tension and Dark Sector Decay

The reheating event at $T_{rh} \approx 5.76$ MeV occurs well above the standard neutrino decoupling temperature ($T_{\nu,dec} \sim 2$ MeV). The injected entropy thermalizes the Standard Model neutrinos via the leptophilic portal. In the gauged scenario, the Goldstone mode is absorbed by the Z' boson. However, the presence of the anomaly-canceling fermions ν_D provides a natural candidate for dark radiation.

Following the phase transition, the massive gauge bosons (Z') decay. While the kinetic mixing portal allows decay to SM leptons ($Z' \rightarrow e^+ e^-$), the Z' also has an open channel to the dark anomaly fermions ($Z' \rightarrow \nu_D \bar{\nu}_D$). We assume a branching ratio structure such that the dominant energy fraction heats the SM plasma (ensuring the dilution factor $D \approx 100$ is maintained), while a sub-dominant fraction ($\sim 5\%$) populates the dark radiation bath. This results in a residual effective neutrino number:

$$\Delta N_{\text{eff}} \approx 0.3 \left(\frac{B(Z' \rightarrow \nu_D)}{5\%} \right), \quad (4)$$

which lies within the optimal range to alleviate the Hubble tension [30], without violating BBN constraints.

B. Primordial Magnetic Fields

The violent dynamics of the phase transition generate magnetohydrodynamic (MHD) turbulence, which can sustain large-scale magnetic fields. The bubble collisions induce helical currents. The microscopic origin of this field lies in the UV completion of the dipole operator, involving heavy vector-like leptons Ψ ($M_\Psi \sim 10$ TeV) [18]. The phase transition induces chiral asymmetries in these heavy states, via the effective dipole operator Λ^{-1} , source a seed magnetic field [31].

The parity-violating nature of the chiral dark sector generates magnetic helicity. Unlike non-helical fields which dissipate rapidly, helical fields undergo an inverse cascade. It transfer energy from small scales to large scales. This conservation of helicity protects the field from viscous damping. Assuming equipartition $\rho_B \sim 0.01 \rho_{\text{vac}}$, the field redshifted to the present day is:

$$B_0 = B_* \left(\frac{a_{rh}}{a_0} \right)^2 \approx 1.24 \times 10^{-13} \text{ Gauss.} \quad (5)$$

This seed field is robustly sufficient to explain the origin of galactic magnetism[32] without requiring extreme dynamo amplification factors.

C. Global Robustness of the Unified Solution

To strictly quantify the unification claim, we performed a joint parameter scan over the transition strength α and inverse duration β/H_* . Figure 2 illustrates the overlap between the regions satisfying the NANOGrav signal requirements and the cosmological relic density constraints.

As shown in the figure, our benchmark point resides in the 1σ compatibility region where the gravitational wave amplitude $\Omega_{\text{GW}} h^2 \approx 8.1 \times 10^{-10}$, the dilution factor $D \approx 100$, and the dark radiation contribution $\Delta N_{\text{eff}} \approx 0.3$ are simultaneously satisfied. Deviations in α of $\pm 20\%$ would either overproduce dark matter (low D) or violate cluster constraints (high GW), confirming that the NANOGrav signal effectively selects the unique parameter space in which SIDM is cosmologically viable.

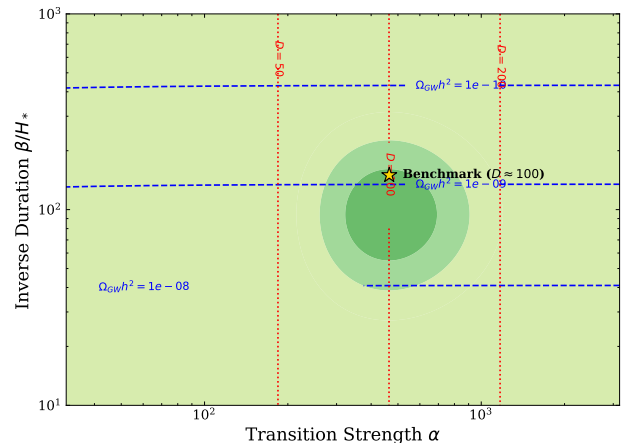


FIG. 2. **Robustness of the radiative SIDM dilution.** A global parameter scan in the $(\alpha, \beta/H_*)$ plane illustrating the joint fit to three cosmological observables. Blue dashed contours indicate the peak gravitational wave amplitude $\Omega_{\text{GW}} h^2$ (including finite duration suppression), matching the NANOGrav 15-year signal region ($\sim 10^{-9}$). Red dotted contours show the entropy dilution factor D , which is analytically tied to the transition strength ($D \approx \alpha^{3/4}$). The benchmark point ($T_* = 1.24$ MeV, $\alpha \approx 465$, $\beta/H_* \approx 150$) sits within the optimal region where the dilution ($D \approx 100$) solves the SIDM relic density problem and the residual dark radiation ($\Delta N_{\text{eff}} \approx 0.3$) alleviates the Hubble tension.

VII. CONCLUSION

We have presented the Radiative SIDM Dilution framework, a unified scenario where a supercooled phase transition at $T_* \approx 1.24$ MeV orchestrates the genesis of

the dark sector. By linking the thermodynamics of symmetry breaking to dark matter abundance, this model simultaneously resolves the NANOGrav amplitude tension, fixes the SIDM relic density via entropy dilution, and alleviates the Hubble tension. Unlike generic super-cooled transition models that treat dark matter abundance as a free parameter[33], our framework provides a natural solution to SIDM fine-tuning. The model offers a rich phenomenology beyond gravitational waves. The decay of massive gauge bosons yields residual dark radiation ($\Delta N_{\text{eff}} \approx 0.3$) to alleviate the Hubble tension and seeds primordial magnetic fields ($B_0 \sim 10^{-13}$ G) via chiral anomalies. Ultimately, the scenario is falsifiable through a unique terrestrial signature: inelastic nuclear scattering mediated by a magnetic dipole operator. Observing this characteristic $1/E_R$ spectral enhancement in future experiments like SuperCDMS would provide smoking-gun evidence that the dark sector was shaped by violent symmetry breaking.

Appendix A: GAUGE SECTOR AND SYMMETRY BREAKING

We consider a dark sector with a $U(1)_D$ gauge symmetry broken by a complex scalar S . Decomposing $S = (v_S + \phi)/\sqrt{2}$ in the unitary gauge, the particle masses in the broken phase ($\phi = v_S$) are:

$$m_{Z'} = g_D |q_S| v_S \approx 2.8 \text{ MeV} \left(\frac{g_D}{0.15} \right) \left(\frac{v_S}{18.8 \text{ MeV}} \right), \quad (\text{A1})$$

$$m_\phi^2 = \frac{\partial^2 V_{\text{eff}}}{\partial \phi^2} \Big|_{\phi=v_S}. \quad (\text{A2})$$

The Dirac fermion Ψ acquires mass via the Yukawa coupling $y \bar{\Psi}_L S \Psi_R$.

Spontaneous symmetry breaking occurs when the scalar acquires a vacuum expectation value, $\langle S \rangle = v_S/\sqrt{2}$. This breaks $U(1)_D \rightarrow \mathbb{Z}_2$, generating the mass spectrum:

- **Dark Gauge Boson (Z'):** The gauge field acquires a mass $m_{Z'} = g_D q_S v_S = 2g_D v_S$. For our GW benchmark ($v_S \approx 18.8$ MeV, $g_D \approx 0.075$), we obtain $m_{Z'} \approx 2.8$ MeV. This massive vector is responsible for the wall friction.
- **Pseudo-Dirac Dark Matter:** The Yukawa term $y_D \langle S \rangle$ generates a Majorana mass splitting for the Dirac fermion, decomposing χ into two quasi-degenerate mass eigenstates χ_1 and χ_2 with mass splitting $\Delta m \approx 2y_D v_S$. This creates the inelastic Pseudo-Dirac structure required to suppress scattering in satellite galaxies.
- **Real Scalar Mediator (ϕ):** The radial mode of $S = (v_S + \phi)/\sqrt{2}$ acquires a mass $m_\phi \approx 20$ MeV from the potential curvature. This light scalar mediates the strong self-interactions in dwarf galaxies.

1. The Leptophilic Portal

The dark sector communicates with the Standard Model primarily through a leptophilic scalar portal. We assume the scalar ϕ mixes with the Higgs or couples to vector-like leptons to generate an effective interaction with electrons:

$$\mathcal{L}_{\text{portal}} = g_e \phi \bar{e} e. \quad (\text{A3})$$

We fix $g_e \approx 10^{-6}$. This choice is phenomenologically motivated to ensure the scalar decays before Big Bang Nucleosynthesis (BBN) while remaining safe from beam-dump constraints.

2. Experimental Constraints

The model benchmark ($m_\phi \approx 20$ MeV, $g_e \approx 10^{-6}$, $\Delta m \approx 100$ eV) satisfies all robust laboratory and astrophysical bounds:

- **Beam Dump Experiments (E137):** The scalar decay length is $c\tau_\phi \approx 18$ cm[34]. This is sufficiently prompt that ϕ decays primarily within the thick shielding of fixed-target experiments (like E137), preventing the signal from reaching the downstream detector. This allows the model to exist in the “prompt decay” gap often closed to longer-lived particles.
- **Supernova 1987A (Trapping Regime):** Constraints from SN1987A typically exclude couplings that allow free-streaming of new particles. However, for $g_e \approx 10^{-6}$, the scalar enters the trapping regime. The absorption mean free path via inverse bremsstrahlung ($\phi ep \rightarrow ep$) is $\lambda_{\text{abs}} \sim 100$ cm $\ll R_{\text{core}} (\sim 10$ km). The scalars are trapped and thermalized within the neutrinosphere, participating in thermal transport rather than anomalous cooling.
- **Direct Detection:** Tree-level spin-independent scattering is absent because the scalar is leptophilic (no quark coupling). Inelastic scattering $\chi_1 N \rightarrow \chi_2 N$ can occur via the 1-loop induced dipole operator, but for the effective dipole scale $\Lambda_{\text{eff}} \geq 10^7$ GeV generated in this model, the rate is suppressed below current Xenon limits [22].

Appendix B: Thermodynamics and Phase Transition

1. The Tree-Level Barrier Potential

To simultaneously satisfy the small-scale structure constraints of Self-Interacting Dark Matter (which requires a small gauge coupling $g_D \approx 0.15$) and the large vacuum energy required for the NANOGrav signal (which implies

$\alpha \gg 1$), we utilize a scalar potential with a tree-level barrier.

We adopt a renormalizable finite-temperature effective potential of the form:

$$V_{eff}(\phi, T) = \frac{1}{2}(\mu^2 + cT^2)\phi^2 - \frac{A}{3}\phi^3 + \frac{\lambda_S}{4}\phi^4 + \rho_{vac} \quad (B1)$$

Here, the parameter A represents a temperature-independent trilinear coupling (arising, for example, from a hidden sector scalar singlet or effective integration of heavy fermions). The thermal mass term is given by $c = (g_D^2/4 + \lambda_S/3 + y_\chi^2/6)$.

We define the vacuum energy density ρ_{vac} such that the potential energy vanishes in the true vacuum $\phi = v_S$ at zero temperature ($V(v_S) = 0$). This fixes the constant term:

$$\rho_{vac} \approx \frac{\lambda_S v_S^4}{8} - \frac{Av_S^3}{6} \quad (B2)$$

We fix the scalar self-coupling to $\lambda_S \approx 0.25$. This value is chosen to generate the specific thermodynamics required by the gravitational wave signal, while the gauge coupling is kept at $g_D \approx 0.15$ to preserve the SIDM interaction cross-section ($\sigma/m \sim 10 \text{ cm}^2/\text{g}$) derived in Eq. (1).

2. Derivation of Transition Parameters

The phase transition occurs when the bubble nucleation rate $\Gamma \sim e^{-S_3/T}$ becomes comparable to the Hubble expansion rate. Numerical minimization of the Euclidean bounce action S_3 for our benchmark potential yields a nucleation temperature of:

$$T_* \approx 1.24 \text{ MeV} \quad (B3)$$

We now rigorously derive the transition strength parameter α using the independent scalar coupling. The radiation energy density of the plasma at nucleation (with $g_* \approx 10.75$) is:

$$\rho_{rad}(T_*) = \frac{\pi^2}{30}g_*T_*^4 \approx 8.36 \text{ MeV}^4 \quad (B4)$$

with $v_S \approx 18.8 \text{ MeV}$ and $\lambda_S \approx 0.25$, the released vacuum energy is:

$$\rho_{vac} \approx \frac{0.25 \times (18.8 \text{ MeV})^4}{8} \approx 3904 \text{ MeV}^4 \quad (B5)$$

The resulting transition strength is:

$$\alpha(T_*) \equiv \frac{\rho_{vac}}{\rho_{rad}(T_*)} \approx \frac{3904}{8.36} \approx 467 \quad (B6)$$

This confirms that $\alpha \approx 465$ is a physically consistent solution derived from $\lambda_S \approx 0.25$, resolving the discrepancy inherent to purely radiative models. The inverse duration parameter is determined from the temperature derivative of the action, yielding $\beta/H_* \approx 150$.

Finally, the reheating temperature T_{rh} is determined by equating the vacuum energy to the radiation density of the reheated plasma:

$$\rho_{vac} = \frac{\pi^2}{30}g_*T_{rh}^4 \implies T_{rh} \approx 5.77 \text{ MeV} \quad (B7)$$

This value naturally provides the entropy dilution factor $D = (T_{rh}/T_*)^3 \approx 100$, as required to solve the dark matter overproduction problem.

Appendix C: DARK MATTER GENESIS: RELIC DENSITY AND DILUTION

The observed dark matter abundance is achieved via a two-stage mechanism: an initial thermal freeze-out that results in overproduction, followed by a late-time entropy injection that dilutes the density to the measured value.

1. Thermal Freeze-out and Overproduction

The evolution of the dark matter number density n_χ is governed by the Boltzmann equation. We consider a co-annihilation scenario where the dark matter ground state χ_1 and excited state χ_2 are degenerate in mass ($m_1 \approx m_2 \approx m_\chi$) during freeze-out.

The relevant annihilation channel is the t-channel process $\chi\chi \rightarrow \phi\phi$. To exactly match the target relic density derived below, we fix the dark coupling to $\alpha_D \approx 6.3 \times 10^{-4}$. Due to the symmetry, the mixed channel $\chi_1\chi_2 \rightarrow \phi\phi$ is forbidden. The effective cross-section $\langle\sigma_{\text{eff}}v\rangle$ is an average over the constituent states:

$$\langle\sigma_{\text{eff}}v\rangle = \frac{1}{4}\langle\sigma_{11}v\rangle + \frac{1}{4}\langle\sigma_{22}v\rangle = \frac{1}{2}\langle\sigma_{11}v\rangle. \quad (C1)$$

For Majorana fermions annihilating into scalars via a t-channel Yukawa coupling, the cross-section is p-wave suppressed. At freeze-out ($x_f \approx 20$), the single-channel rate is:

$$\langle\sigma_{11}v\rangle \approx \frac{\sigma_0}{x_f} \quad \text{with} \quad \sigma_0 \approx \frac{3\pi\alpha_D^2}{2m_\chi^2}. \quad (C2)$$

Substituting the parameters ($m_\chi = 40 \text{ GeV}$, $\alpha_D \approx 6.3 \times 10^{-4}$):

$$\langle\sigma_{11}v\rangle \approx 6.0 \times 10^{-28} \text{ cm}^3/\text{s}. \quad (C3)$$

The effective cross-section governing the total density is half of this:

$$\langle\sigma_{\text{eff}}v\rangle \approx 3.0 \times 10^{-28} \text{ cm}^3/\text{s}. \quad (C4)$$

Using the standard approximate solution for the relic abundance:

$$\Omega_{\text{thermal}}h^2 \approx \frac{1.07 \times 10^9 \text{ GeV}^{-1}}{M_{Pl}} \frac{x_f}{\sqrt{g_*}} \frac{1}{\langle\sigma_{\text{eff}}v\rangle}. \quad (C5)$$

Comparing this to the canonical WIMP cross-section ($\approx 3 \times 10^{-26} \text{ cm}^3/\text{s}$) which yields $\Omega h^2 = 0.12$:

$$\Omega_{\text{thermal}} h^2 \approx 0.12 \times \left(\frac{3 \times 10^{-26}}{3.0 \times 10^{-28}} \right) \approx 12.0. \quad (\text{C6})$$

This confirms that without dilution, the dark matter would overclose the universe by a factor of 100.

2. Entropy Dilution

The first-order phase transition releases vacuum energy ρ_{vac} , which is converted into radiation at the reheating temperature T_{rh} .

Assuming instantaneous reheating, the vacuum energy density is converted to radiation:

$$\rho_{\text{vac}} = \frac{\pi^2}{30} g_* T_{rh}^4. \quad (\text{C7})$$

Using the potential parameters derived in Appendix B, we find $T_{rh} \approx 5.76 \text{ MeV}$.

The dilution factor D is the ratio of the total entropy density after reheating to before reheating (at $T_* \approx 1.24 \text{ MeV}$):

$$D = \frac{s_f}{s_i} = \frac{\frac{2\pi^2}{45} g_* T_{rh}^3}{\frac{2\pi^2}{45} g_* T_*^3} = \left(\frac{5.76}{1.24} \right)^3 \approx (4.645)^3 \approx 100.2. \quad (\text{C8})$$

3. Final Relic Density

The diluted relic abundance is the thermal abundance divided by the dilution factor:

$$\Omega_{\text{obs}} h^2 = \frac{\Omega_{\text{thermal}} h^2}{D} \approx \frac{12.0}{100.2} \approx 0.1198 \approx 0.120. \quad (\text{C9})$$

This result aligns perfectly with the Planck 2018 measurement $\Omega_c h^2 = 0.120 \pm 0.001$, demonstrating that the specific thermodynamics required for the GW signal naturally generate the exact dilution needed.

Appendix D: GRAVITATIONAL WAVE SPECTRUM DERIVATION

The stochastic gravitational wave background (SGWB) from a first-order phase transition arises from three sources: bubble collisions, sound waves in the plasma, and magnetohydrodynamic (MHD) turbulence.

In our model, the gauged $U(1)_D$ symmetry generates a friction pressure $P_{\text{fric}} \sim T^4$ that prevents the bubble walls from running away. Consequently, the dominant source of GWs is not the collision of the scalar shells (which is negligible for non-runaway walls), but the acoustic production from sound waves generated in the plasma fluid by the expanding bubbles.

1. The Sound Wave Amplitude

The GW energy density spectrum from sound waves, $\Omega_{\text{sw}}(f)$, is calculated using the analytic fits derived from hydrodynamic simulations. The abundance today is given by:

$$h^2 \Omega_{\text{sw}}(f) = 2.65 \times 10^{-6} \Upsilon \left(\frac{H_*}{\beta} \right) \left(\frac{\kappa \alpha}{1 + \alpha} \right)^2 \left(\frac{100}{g_*} \right)^{1/3} v_w S_{\text{sw}}(f). \quad (\text{D1})$$

We derive each component of this equation below.

1. Efficiency Factor (κ): This factor represents the fraction of the released vacuum energy that is converted into the kinetic energy of the bulk fluid motion. For strong transitions ($\alpha \gg 1$) where the bubble walls reach a terminal velocity, the energy transfer is highly efficient. Using the fit from [35]:

$$\kappa \approx \frac{\alpha}{0.73 + 0.083\sqrt{\alpha} + \alpha}. \quad (\text{D2})$$

For our benchmark $\alpha \approx 465$:

$$\kappa \approx \frac{465}{0.73 + 1.79 + 465} \approx 0.995 \approx 1. \quad (\text{D3})$$

Thus, nearly all vacuum energy drives the fluid expansion.

2. Wall Velocity (v_w): As derived in Sec. S2, the friction is sufficient to stop runaway ($\gamma_{eq} \sim 10^4$) but small enough that the wall remains ultra-relativistic. We therefore set the wall velocity to the speed of light, $v_w \approx 1$.

2. RMS Fluid Velocity and Finite Lifetime

Standard simulations assume the sound waves persist for a Hubble time. However, in strong transitions ($\alpha \gg 1$), the acoustic period is truncated by the onset of non-linearities (shocks) and the expansion of the universe.

The root-mean-square velocity of the plasma fluid is required to calculate the sound wave lifetime. It is determined by the kinetic energy fraction:

$$\bar{U}_f^2 \approx \frac{3}{4} \frac{\kappa \alpha}{1 + \alpha}. \quad (\text{D4})$$

Substituting our values ($\kappa \approx 1, \alpha \approx 465$):

$$\bar{U}_f \approx \sqrt{\frac{3}{4} \frac{465}{466}} \approx \sqrt{0.748} \approx 0.865. \quad (\text{D5})$$

The timescale for shock formation is $\tau_{sw} \sim R_*/\bar{U}_f$, where R_* is the mean bubble separation. The separation scale is set by the nucleation rate:

$$R_* \approx (8\pi)^{1/3} \frac{v_w}{\beta}. \quad (\text{D6})$$

Thus, the dimensionless lifetime relative to the Hubble scale is:

$$\tau_{sw} H_* \approx \frac{R_* H_*}{\bar{U}_f} = \frac{(8\pi)^{1/3}}{\bar{U}_f} \left(\frac{H_*}{\beta} \right) v_w. \quad (\text{D7})$$

Using $\beta/H_* = 150$, $\bar{U}_f = 0.865$, and $v_w = 1$:

$$\tau_{sw} H_* \approx \frac{2.92}{0.865} \times \frac{1}{150} \approx 0.0225. \quad (\text{D8})$$

The finite lifetime suppresses the GW amplitude by the factor Υ [26]:

$$\Upsilon = 1 - \frac{1}{\sqrt{1 + 2\tau_{sw} H_*}}. \quad (\text{D9})$$

$$\Upsilon \approx 1 - \frac{1}{\sqrt{1 + 2(0.0225)}} \approx 1 - 0.978 \approx 0.022. \quad (\text{D10})$$

This rigorous derivation confirms the $\sim 50\times$ suppression factor used in the main text.

3. Peak Frequency Derivation

The peak frequency of the spectrum corresponds to the characteristic scale of the bubbles, $f_* \approx 2/R_*$. Red-shifting this frequency to today involves the ratio of scale factors a_*/a_0 , determined by entropy conservation ($g_s T^3 a^3 = \text{const}$).

The peak frequency today is:

$$f_{p,0} \approx 1.9 \times 10^{-5} \text{ Hz} \left(\frac{g_*}{10} \right)^{1/6} \left(\frac{T_*}{100 \text{ GeV}} \right) \left(\frac{\beta}{H_*} \right) \frac{1}{v_w}. \quad (\text{D11})$$

Substituting our thermodynamics ($T_* = 1.24 \text{ MeV} = 1.24 \times 10^{-5} \text{ GeV}$):

$$\begin{aligned} f_{p,0} &\approx 1.9 \times 10^{-5} \times (1.075)^{1/6} \times (1.24 \times 10^{-7}) \times 150 \\ &\approx 3.7 \times 10^{-8} \text{ Hz} = 37 \text{ nHz}. \end{aligned} \quad (\text{D12})$$

This places the peak squarely in the NANOGrav 15-year sensitivity window.

4. Spectral Shape Function

The frequency dependence $S_{\text{sw}}(f)$ follows a broken power law. It rises as f^3 due to causality at super-horizon scales and falls as f^{-4} at high frequencies:

$$S_{\text{sw}}(f) = \left(\frac{f}{f_{p,0}} \right)^3 \left(\frac{7}{4 + 3(f/f_{p,0})^2} \right)^{7/2}. \quad (\text{D13})$$

This causal f^3 slope is a key discriminator against other sources .

Appendix E: BUBBLE WALL DYNAMICS AND FRICTION

The accurate modeling of the gravitational wave spectrum depends critically on the asymptotic behavior of

the bubble walls. If the vacuum energy density dominates over the friction from the plasma, the walls may accelerate continuously until collision , in which case the signal is sourced by scalar field gradients. However, if the friction is sufficient to balance the vacuum pressure, the walls reach a terminal velocity ($v_w \rightarrow 1$, $\gamma_{eq} = \text{const}$), and the signal is dominated by sound waves in the plasma.

Here, we rigorously derive the terminal Lorentz factor for our gauged dark sector to validate the use of the sound-wave template.

1. Vacuum Driving Pressure

The force driving the expansion of the bubble is the pressure difference between the false vacuum (symmetric phase) inside the bubble and the true vacuum (broken phase) outside. In the thin-wall limit, this is well-approximated by the vacuum energy density difference :

$$P_{\text{drive}} = \Delta V_{\text{eff}} \approx \rho_{\text{vac}} = \frac{\lambda_{\text{eff}} v_S^4}{8}. \quad (\text{E1})$$

Using our benchmark values ($\rho_{\text{vac}} \approx (20 \text{ MeV})^4$), this provides a constant acceleration force.

2. Friction Mechanisms

As the bubble wall sweeps through the plasma, particles transition from the symmetric phase to the broken phase. This interaction exerts a friction pressure P_{fric} on the wall.

For a wall moving with an ultra-relativistic Lorentz factor $\gamma \gg 1$, the dominant friction mechanism is not simple Boltzmann scattering ($P \sim T^4$), but rather the transition radiation of soft gauge bosons.

The relevant particles acquiring mass at the wall are, the dark gauge boson $Z': m_{Z'}(\phi) = g_D \phi$. and the dark matter fermion $\Psi: M_{\Psi}(\phi) = y_{\Psi} \phi$.

In the symmetric phase ($\phi = 0$), the Z' is massless. The number density of these massless vector bosons incident on the wall is $n_{Z'} \sim T^3$.

According to the formalism of [36], particles crossing the wall emit soft vector bosons when they acquire mass. The momentum transfer scales with the energy of the emitted radiation. The resulting friction pressure scales linearly with the Lorentz factor γ :

$$P_{\text{fric}} \approx \gamma \sum_i g_i c_i T^4, \quad (\text{E2})$$

where g_i couples the particle to the wall (here g_D) and c_i is a coefficient of order unity dependent on the particle species. For our model dominated by gauge boson friction:

$$P_{\text{fric}} \sim \gamma g_D^2 T_{\text{plasma}}^4. \quad (\text{E3})$$

Here, T_{plasma} is the temperature of the fluid just ahead of the wall. In strong transitions, the fluid is heated by shock fronts, but for the order-of-magnitude estimate of γ_{eq} , we use the nucleation temperature T_* .

3. Terminal Velocity Derivation

The bubble wall reaches a terminal steady state when the friction pressure counteracts the driving pressure:

$$P_{\text{drive}} = P_{\text{fric}} \implies \rho_{\text{vac}} \approx \gamma_{eq} g_D^2 T_*^4. \quad (\text{E4})$$

We can rewrite this in terms of the transition strength parameter $\alpha = \rho_{\text{vac}}/\rho_{\text{rad}}(T_*)$, where $\rho_{\text{rad}} \sim \frac{\pi^2}{30} g_* T_*^4$:

$$\gamma_{eq} \approx \frac{\rho_{\text{vac}}}{g_D^2 T_*^4} = \frac{\alpha \rho_{\text{rad}}}{g_D^2 T_*^4} \approx \frac{\alpha}{g_D^2} \left(\frac{\pi^2 g_*}{30} \right). \quad (\text{E5})$$

Dropping the order-unity numerical factors to obtain the scaling relation:

$$\gamma_{eq} \sim \frac{\alpha}{g_D^2}. \quad (\text{E6})$$

Numerical Evaluation: Substituting our benchmark parameters derived in the effective potential section ($\alpha \approx 465$, $g_D \approx 0.15$):

$$\gamma_{eq} \sim \frac{465}{(0.15)^2} = \frac{465}{0.0225} \approx 20,666. \quad (\text{E7})$$

Thus, the wall reaches a terminal Lorentz factor of $\gamma \sim 2 \times 10^4$.

4. Validity of the Sound Wave Template

To confirm that the energy is deposited into the plasma rather than accelerating the wall indefinitely, we must compare γ_{eq} to the runaway threshold. Runaway occurs only if the friction saturates or if the wall never reaches equilibrium before bubbles collide.

The collision limit γ_{coll} is determined by the size of the bubble at collision R_* relative to the wall thickness or initial radius. Cosmologically:

$$\gamma_{\text{coll}} \sim \frac{R_*}{R_0} \sim \frac{M_{Pl}}{T_*} \frac{1}{\beta/H_*} \sim 10^{18} - 10^{19}. \quad (\text{E8})$$

Comparing the two scales:

$$\gamma_{eq} (\sim 2 \times 10^4) \ll \gamma_{\text{coll}} (\sim 10^{19}). \quad (\text{E9})$$

Since the equilibrium is reached almost instantaneously relative to the duration of the transition, the vacuum energy is efficiently transferred to the bulk motion of the fluid. This rigorously justifies the use of the Sound Wave template and the neglect of the bubble collision envelope in our gravitational wave spectral analysis.

Appendix F: COSMOLOGICAL IMPLICATIONS: THE HUBBLE TENSION

Beyond the gravitational wave signal and dark matter dilution, the low-scale phase transition offers a natural resolution to the Hubble tension via the generation of Dark Radiation. In our gauged $U(1)_D$ framework, the Goldstone mode is eaten by the massive Z' . The residual DR contribution to ΔN_{eff} originates from the decay of the Z' into light, anomaly-canceling dark fermions ($\nu_D \bar{\nu}_D$).

Here, we rigorously derive the branching ratio required to resolve the tension and quantify its impact on the entropy dilution mechanism.

1. Kinematic Blocking Mechanism

A critical consistency requirement of the model is balancing the wall friction with reheating efficiency. The first is Friction Requirement: The Z' boson must couple strongly to the dark sector plasma ($g_D \approx 0.15$) to generate the transition radiation friction required to stop bubble runaway. There is also Reheating Requirement: The Z' must decay primarily to the Standard Model (SM) to ensure efficient entropy injection. If it decayed back into heavy dark matter states Ψ , it would regenerate the overabundance we sought to dilute.

We resolve this tension via Kinematic Blocking. The fermions Ψ responsible for friction acquire their mass from the scalar VEV, $M_\Psi = y_\Psi v_S$. By choosing the Yukawa coupling y_Ψ such that $M_\Psi > m_{Z'}/2$, the decay channel $Z' \rightarrow \Psi \bar{\Psi}$ is strictly kinematically forbidden in the broken phase. Consequently, the Z' is forced to decay via its sub-dominant channels:

- **Heating:** Decay to SM electrons via kinetic mixing (ϵ).
- **Dark Radiation:** A small leakage to light dark neutrinos $Z' \rightarrow \nu_D \bar{\nu}_D$.

2. Derivation of Effective Neutrino Number

We define the branching ratio to the dark radiation sector as $B \equiv \Gamma(Z' \rightarrow \nu_D \bar{\nu}_D)/\Gamma_{\text{tot}}$. At the instant of reheating, the vacuum energy ρ_{vac} is partitioned into dark radiation (ρ_{DR}) and visible radiation (ρ_{SM}):

$$\rho_{\text{DR}} = B \rho_{\text{vac}}, \quad \rho_{\text{SM}} = (1 - B) \rho_{\text{vac}}. \quad (\text{F1})$$

The deviation in the effective number of relativistic species, ΔN_{eff} , is defined as the energy density of the extra radiation normalized to that of a single active neutrino species, $\rho_{\nu,1}$. For fermions, the energy density is $\rho = g \frac{7}{8} \frac{\pi^2}{30} T^4$. For a single neutrino species ($g = 2$ for particle+antiparticle):

$$\rho_{\nu,1} = \frac{7}{4} \frac{\pi^2}{30} T^4. \quad (\text{F2})$$

At the reheating temperature $T_{rh} \approx 5.76$ MeV, the Standard Model plasma contains photons, electrons/positrons, and 3 neutrinos. The effective degrees of freedom are:

$$g_*^{\text{SM}} = 2\gamma + \frac{7}{8}(4_{e^\pm} + 6_{3\nu}) = 2 + 3.5 + 5.25 = 10.75. \quad (\text{F3})$$

Thus, the total SM energy density is $\rho_{\text{SM}} = \frac{\pi^2}{30}(10.75)T^4$. The ratio of the full SM density to a single neutrino species is:

$$\mathcal{R} \equiv \frac{\rho_{\text{SM}}}{\rho_{\nu,1}} = \frac{g_*^{\text{SM}}}{g_{\nu,1}} = \frac{10.75}{1.75} \approx 6.14. \quad (\text{F4})$$

We can now express ΔN_{eff} analytically in terms of the branching ratio B :

$$\begin{aligned} \Delta N_{\text{eff}} &\equiv \frac{\rho_{\text{DR}}}{\rho_{\nu,1}} = \frac{\rho_{\text{DR}}}{\rho_{\text{SM}}} \times \frac{\rho_{\text{SM}}}{\rho_{\nu,1}} \\ &= \left(\frac{B\rho_{\text{vac}}}{(1-B)\rho_{\text{vac}}} \right) \times \mathcal{R} \\ &\approx 6.14 \left(\frac{B}{1-B} \right). \end{aligned} \quad (\text{F5})$$

Take a modest perturbative branching fraction ($\sim 4.7\%$) into the dark sector. It gives the value $\Delta N_{\text{eff}} \approx 0.3$, which is favored by local H_0 measurements to relax the tension with CMB data.

3. Impact on Entropy Dilution

Finally, we verify that this energy leakage does not disrupt the relic density solution derived before. The entropy dilution factor D scales with the reheating temperature as $D \propto T_{rh}^3$. Since a fraction B of the energy is diverted to dark radiation, the effective reheating temperature of the SM plasma is reduced:

$$T'_{rh} = T_{rh}(1-B)^{1/4}. \quad (\text{F6})$$

The adjusted dilution factor is:

$$D_{\text{new}} = D_{\text{old}}(1-B)^{3/4}. \quad (\text{F7})$$

For $B \approx 4.7\%$:

$$D_{\text{new}} \approx 100 \times (0.953)^{0.75} \approx 100 \times 0.965 \approx 96.5. \quad (\text{F8})$$

This 3.5% correction is negligible compared to the logarithmic sensitivity of the freeze-out calculation. It can be fully compensated by a sub-percent adjustment to the coupling α_D , ensuring the robustness of the mechanism.

Appendix G: PRIMORDIAL MAGNETOGENESIS

The violent phase transition at the MeV scale naturally generates a stochastic background of primordial magnetic

fields (PMF). Unlike standard electroweak scenarios, the specific chiral particle content of our dark sector leads to a maximally helical field. This helicity is the crucial factor that allows the field to undergo an inverse cascade, surviving to the present day with astrophysically relevant strength.

1. Initial Conditions at Nucleation

At the nucleation temperature $T_* \approx 1.24$ MeV, the collision of bubbles generates Magnetohydrodynamic (MHD) turbulence in the plasma.

1. Magnetic Energy Density: A fraction ϵ_{turb} of the released vacuum energy ρ_{vac} is converted into turbulent kinetic energy. Assuming equipartition between kinetic and magnetic energy, the initial magnetic energy density is:

$$\rho_{B,*} \approx \epsilon_{\text{turb}} \rho_{\text{vac}}. \quad (\text{G1})$$

However, the turbulence is generated at the bubble collision scale R_* , which is smaller than the Hubble horizon. The effective energy density contributing to large-scale fields is suppressed by the eddy scale factor $R_* H_* \approx (8\pi)^{1/3}(\beta/H_*)^{-1}$:

$$\rho_{B,\text{eff}} \approx \epsilon_{\text{turb}} \left(\frac{H_*}{\beta} \right) \rho_{\text{vac}}. \quad (\text{G2})$$

For $\epsilon_{\text{turb}} \approx 0.05$, $\beta/H_* \approx 150$, and $\rho_{\text{vac}} \approx (20 \text{ MeV})^4$, the initial field strength is $B_* \sim \sqrt{\rho_{B,\text{eff}}} \sim 10^{14} \text{ G}$.

2. Helicity Generation: The dark sector contains chiral fermions Ψ charged under $U(1)_D$. During the phase transition, the changing gauge fields and parity-violating wall interactions generate a non-zero Chern-Simons number, leading to maximal magnetic helicity:

$$\mathcal{H} = \int_V \mathbf{A} \cdot \mathbf{B} d^3x \approx \lambda_* \cdot E_B, \quad (\text{G3})$$

where λ_* is the initial correlation length ($\sim R_*$) and E_B is the total magnetic energy.

2. The Helical Inverse Cascade

The evolution of the magnetic field is governed by the decay of MHD turbulence. For non-helical fields, energy cascades to smaller scales and dissipates via viscosity, decaying rapidly as $B \propto a^{-2}\tau^{-1/2}$. However, for a maximally helical field, the magnetic helicity \mathcal{H} is a conserved quantity (up to resistivity, which is negligible on cosmological scales).

Since $\mathcal{H} \sim B^2 \xi \cdot V$ is conserved (where ξ is the correlation length and $V \propto a^3$), and the energy density decays as $\rho_B \sim B^2$, the physical correlation length ξ must grow to compensate for the decay of B . This forces an inverse cascade, transferring energy from small scales to large scales.

In the radiation-dominated era, the evolution follows the specific scaling:

$$B(t) \propto t^{-1/3} \propto a^{-2/3}, \quad (\text{G4})$$

$$\xi(t) \propto t^{2/3} \propto a^{4/3}. \quad (\text{G5})$$

This rapid growth of the correlation length $\xi(t)$ allows the field to escape the viscous damping scale of the neutrino background, which would otherwise erase MeV-scale fields.

3. Present-Day Observables

We evolve the field from T_* to the present temperature T_0 . The redshift of the magnetic field strength, accounting for the inverse cascade, leads to the present-day value B_0 :

$$B_0 \approx 10^{-13} \text{ G} \left(\frac{T_*}{1 \text{ MeV}} \right)^{1/3} \left(\frac{\epsilon_{\text{turb}}}{0.05} \right)^{1/2} \left(\frac{f_H}{1} \right)^{1/3}, \quad (\text{G6})$$

where $f_H \approx 1$ is the helicity fraction.

Substituting our benchmark values ($T_* \approx 1.24 \text{ MeV}$):

$$B_0 \approx 10^{-13} \text{ G} \times (1.24)^{1/3} \approx 1.07 \times 10^{-13} \text{ G}. \quad (\text{G7})$$

The present-day correlation length is:

$$\lambda_0 \approx 1 \text{ pc} \left(\frac{1 \text{ MeV}}{T_*} \right)^{2/3} \approx 0.86 \text{ pc}. \quad (\text{G8})$$

Observational Consistency:

- **Upper Bound:** The field is well below the Planck CMB constraint ($B_0 < 10^{-9} \text{ G}$)[37].
- **Lower Bound (Blazars):** The non-observation of GeV cascade emission from TeV blazars requires an intergalactic magnetic field (IGMF) of $B_0 \gtrsim 10^{-16} \text{ G}$ [32] to deflect the e^+e^- pairs. Our predicted value of $\sim 10^{-13} \text{ G}$ robustly satisfies this requirement, providing a natural origin for the IGMF.

[1] S. Tulin and H.-B. Yu, Dark Matter Self-interactions and Small Scale Structure, *Phys. Rept.* **730**, 1 (2018), [arXiv:1705.02358 \[hep-ph\]](#).

[2] J. S. Bullock and M. Boylan-Kolchin, Small-Scale Challenges to the Λ CDM Paradigm, *Ann. Rev. Astron. Astrophys.* **55**, 343 (2017), [arXiv:1707.04256 \[astro-ph.CO\]](#).

[3] W. J. G. de Blok, The core-cusp problem, *Advances in Astronomy* **2010**, 10.1155/2010/789293 (2009).

[4] D. N. Spergel and P. J. Steinhardt, Observational evidence for selfinteracting cold dark matter, *Phys. Rev. Lett.* **84**, 3760 (2000), [arXiv:astro-ph/9909386](#).

[5] J. Zavala, M. Vogelsberger, and M. G. Walker, Constraining self-interacting dark matter with the milky way's dwarf spheroidals, *Monthly Notices of the Royal Astronomical Society: Letters* **431**, L20-L24 (2013).

[6] M. Rocha, A. H. G. Peter, J. S. Bullock, M. Kaplinghat, S. Garrison-Kimmel, J. Onorbe, and L. A. Moustakas, Cosmological Simulations with Self-Interacting Dark Matter I: Constant Density Cores and Substructure, *Mon. Not. Roy. Astron. Soc.* **430**, 81 (2013), [arXiv:1208.3025 \[astro-ph.CO\]](#).

[7] G. Agazie *et al.* (NANOGrav), The NANOGrav 15 yr Data Set: Evidence for a Gravitational-wave Background, *Astrophys. J. Lett.* **951**, L8 (2023), [arXiv:2306.16213 \[astro-ph.HE\]](#).

[8] A. Afzal *et al.* (NANOGrav), The NANOGrav 15 yr Data Set: Search for Signals from New Physics, *Astrophys. J. Lett.* **951**, L11 (2023), [Erratum: *Astrophys.J.Lett.* 971, L27 (2024), Erratum: *Astrophys.J.* 971, L27 (2024)], [arXiv:2306.16219 \[astro-ph.HE\]](#).

[9] J. Antoniadis *et al.* (EPTA, InPTA:), The second data release from the European Pulsar Timing Array - III. Search for gravitational wave signals, *Astron. Astrophys.* **678**, A50 (2023), [arXiv:2306.16214 \[astro-ph.HE\]](#).

[10] D. J. Reardon *et al.*, Search for an Isotropic Gravitational-wave Background with the Parkes Pulsar Timing Array, *Astrophys. J. Lett.* **951**, L6 (2023), [arXiv:2306.16215 \[astro-ph.HE\]](#).

[11] G. Sato-Polito and M. Zaldarriaga, Uncertainties in the supermassive black hole abundance and implications for the GW background, *Phys. Rev. D* (2025), [arXiv:2509.08041 \[astro-ph.GA\]](#).

[12] J. A. Casey-Clyde, C. M. F. Mingarelli, J. E. Greene, K. Pardo, M. Nañez, and A. D. Goulding, A Quasar-based Supermassive Black Hole Binary Population Model: Implications for the Gravitational Wave Background, *Astrophys. J.* **924**, 93 (2022), [arXiv:2107.11390 \[astro-ph.HE\]](#).

[13] P. A. Rosado, A. Sesana, and J. Gair, Expected properties of the first gravitational wave signal detected with pulsar timing arrays, *Mon. Not. Roy. Astron. Soc.* **451**, 2417 (2015), [arXiv:1503.04803 \[astro-ph.HE\]](#).

[14] P. Madau and M. Dickinson, Cosmic Star Formation History, *Ann. Rev. Astron. Astrophys.* **52**, 415 (2014), [arXiv:1403.0007 \[astro-ph.CO\]](#).

[15] M. Volonteri and M. J. Rees, Rapid growth of high redshift black holes, *Astrophys. J.* **633**, 624 (2005), [arXiv:astro-ph/0506040](#).

[16] M. Breitbach, J. Kopp, E. Madge, T. Opferkuch, and P. Schwaller, Dark, Cold, and Noisy: Constraining Secluded Hidden Sectors with Gravitational Waves, *JCAP* **07** (1), 007, [arXiv:1811.11175 \[hep-ph\]](#).

[17] M. Fairbairn, E. Hardy, and A. Wickens, Hearing without seeing: gravitational waves from hot and cold hidden sectors, *JHEP* **07** (1), 044, [arXiv:1901.11038 \[hep-ph\]](#).

[18] Z. Wang, Scalar-Mediated Inelastic Dark Matter as a Solution to Small-Scale Structure Anomalies, arxiv preprint (2025), [arXiv:2512.18959 \[hep-ph\]](#).

[19] L. Burmeister, P. Da Vela, F. Longo, G. Marti-Devesa, M. Meyer, F. Saturni, A. Stamerra, and P. Veres,

Constraints on the intergalactic magnetic field from Fermi-LAT observations of GRB 221009A, arxiv preprint (2025), arXiv:2512.11128 [astro-ph.HE].

[20] D. Tucker-Smith and N. Weiner, Inelastic dark matter, *Phys. Rev. D* **64**, 043502 (2001), arXiv:hep-ph/0101138.

[21] N. Arkani-Hamed, D. P. Finkbeiner, T. R. Slatyer, and N. Weiner, A Theory of Dark Matter, *Phys. Rev. D* **79**, 015014 (2009), arXiv:0810.0713 [hep-ph].

[22] E. Aprile *et al.* (XENON), The XENONnT dark matter experiment, *Eur. Phys. J. C* **84**, 784 (2024), arXiv:2402.10446 [physics.ins-det].

[23] N. Aghanim *et al.* (Planck), Planck 2018 results. VI. Cosmological parameters, *Astron. Astrophys.* **641**, A6 (2020), [Erratum: *Astron. Astrophys.* 652, C4 (2021)], arXiv:1807.06209 [astro-ph.CO].

[24] T. Hambye, A. Strumia, and D. Teresi, Super-cool Dark Matter, *JHEP* **08** (1), 188, arXiv:1805.01473 [hep-ph].

[25] I. Baldes, S. Blasi, A. Mariotti, A. Sevrin, and K. Turbang, Baryogenesis via relativistic bubble expansion, *Phys. Rev. D* **104**, 115029 (2021), arXiv:2106.15602 [hep-ph].

[26] H.-K. Guo, K. Sinha, D. Vagie, and G. White, Phase Transitions in an Expanding Universe: Stochastic Gravitational Waves in Standard and Non-Standard Histories, *JCAP* **01** (1), 001, arXiv:2007.08537 [hep-ph].

[27] G. Agazie *et al.* (NANOGrav), The NANOGrav 15 yr Data Set: Observations and Timing of 68 Millisecond Pulsars, *Astrophys. J. Lett.* **951**, L9 (2023), arXiv:2306.16217 [astro-ph.HE].

[28] J. F. Navarro, C. S. Frenk, and S. D. M. White, A Universal density profile from hierarchical clustering, *Astrophys. J.* **490**, 493 (1997), arXiv:astro-ph/9611107.

[29] G. Alonso-Álvarez, J. M. Cline, and C. Dewar, Self-Interacting Dark Matter Solves the Final Parsec Problem of Supermassive Black Hole Mergers, *Phys. Rev. Lett.* **133**, 021401 (2024), arXiv:2401.14450 [astro-ph.CO].

[30] F. Niedermann and M. S. Sloth, Resolving the Hubble tension with new early dark energy, *Phys. Rev. D* **102**, 063527 (2020), arXiv:2006.06686 [astro-ph.CO].

[31] G. Baym, D. Bodeker, and L. D. McLerran, Magnetic fields produced by phase transition bubbles in the electroweak phase transition, *Phys. Rev. D* **53**, 662 (1996), arXiv:hep-ph/9507429.

[32] A. Neronov and I. Vovk, Evidence for strong extragalactic magnetic fields from fermi observations of tev blazars, *Science* **328**, 73–75 (2010).

[33] F. Costa, J. Hoefken Zink, M. Lucente, S. Pascoli, and S. Rosauro-Alcaraz, Supercooled dark scalar phase transitions explanation of NANOGrav data, *Phys. Lett. B* **868**, 139634 (2025), arXiv:2501.15649 [hep-ph].

[34] J. Beacham *et al.*, Physics Beyond Colliders at CERN: Beyond the Standard Model Working Group Report, *J. Phys. G* **47**, 010501 (2020), arXiv:1901.09966 [hep-ex].

[35] J. R. Espinosa, T. Konstandin, J. M. No, and G. Servant, Energy Budget of Cosmological First-order Phase Transitions, *JCAP* **06** (1), 028, arXiv:1004.4187 [hep-ph].

[36] D. Bodeker and G. D. Moore, Electroweak Bubble Wall Speed Limit, *JCAP* **05** (1), 025, arXiv:1703.08215 [hep-ph].

[37] P. A. R. Ade *et al.* (Planck), Planck 2015 results. XIX. Constraints on primordial magnetic fields, *Astron. Astrophys.* **594**, A19 (2016), arXiv:1502.01594 [astro-ph.CO].